

CORNELL UNIVERSITY LIBRARY

Subscriber access provided by CORNELL UNIVERSITY LIBRARY

Surfaces, Interfaces, and Applications

Single Particle Investigation of Environmental Redox Processes of Arsenic on Cerium Oxide Nanoparticles by Collision Electrochemistry

Anahita Karimi, Silvana Andreescu, and Daniel Andreescu

ACS Appl. Mater. Interfaces, Just Accepted Manuscript • DOI: 10.1021/acsami.9b05234 • Publication Date (Web): 13 Jun 2019

Downloaded from http://pubs.acs.org on June 24, 2019

Just Accepted

"Just Accepted" manuscripts have been peer-reviewed and accepted for publication. They are posted online prior to technical editing, formatting for publication and author proofing. The American Chemical Society provides "Just Accepted" as a service to the research community to expedite the dissemination of scientific material as soon as possible after acceptance. "Just Accepted" manuscripts appear in full in PDF format accompanied by an HTML abstract. "Just Accepted" manuscripts have been fully peer reviewed, but should not be considered the official version of record. They are citable by the Digital Object Identifier (DOI®). "Just Accepted" is an optional service offered to authors. Therefore, the "Just Accepted" Web site may not include all articles that will be published in the journal. After a manuscript is technically edited and formatted, it will be removed from the "Just Accepted" Web site and published as an ASAP article. Note that technical editing may introduce minor changes to the manuscript text and/or graphics which could affect content, and all legal disclaimers and ethical guidelines that apply to the journal pertain. ACS cannot be held responsible for errors or consequences arising from the use of information contained in these "Just Accepted" manuscripts.

Single Particle Investigation of Environmental Redox Processes of Arsenic on Cerium Oxide Nanoparticles by Collision Electrochemistry

Anahita Karimi, Silvana Andreescu and Daniel Andreescu*

Department of Chemistry and Biomolecular Science, Clarkson University, Potsdam, NY, 13699-5810, USA.

E-mail: dandrees@clarkson.edu; Fax: +(315) 268 6610; Tel: +(315) 268 2394

KEYWORDS: arsenic, single nanoparticle collision electrochemistry (SPCE), environmental redox processes, cerium oxide

ABSTRACT

Quantification of chemical reactions of nanoparticles (NPs) and their interaction with contaminants is a fundamental need to the understanding of chemical reactivity and surface chemistry of NPs released into the environment. Herein, we propose a novel strategy employing single particle electrochemistry showing that it is possible to measure reactivity, speciation and loading of As3+ on individual NPs, using cerium oxide (CeO2) as a model system. We demonstrate that redox reactions and adsorption processes can be electrochemically quantified with high sensitivity via the oxidation of As3+ to As5+ at 0.8V vs. Ag/AgCl or the reduction of As³⁺ to As⁰ at -0.3V (vs. Ag/AgCl) generated by collisions of single particles at an ultramicroelectrode (UME). Using collision electrochemistry, As³⁺ concentrations were determined in basic conditions showing a maximum adsorption capacity at pH 8. In acidic environments (pH<4), a small fraction of As³⁺ was oxidized to As⁵⁺ by surface Ce⁴⁺ and further adsorbed onto the CeO₂ surface as a As⁵⁺ bidentate complex. The frequency of current spikes (oxidative or reductive) was proportional to the concentration of As3+ accumulated onto the NPs and was found representative of the As3+ concentration in solution. Given its sensitivity and speciation capability, the method can find many applications in the analytical, materials and environmental chemistry fields where there is a need to quantify the reactivity and surface interactions of NPs. This is the first study demonstrating the capability of single particle collision electrochemistry to monitor the interaction of heavy metal ions with metal oxide NPs. This knowledge is critical to the fundamental understanding of the risks associated with the release of NPs into the environment, for their safe implementation and practical use.

INTRODUCTION

The increasing use of engineered nanomaterials in commercial applications in the electronics, biomedical and agricultural fields has resulted in a significant release of NPs into the environment. Given the wide diversity of NP types and the limitations of currently used characterization methods, a comprehensive analysis of the chemical reactivity at the particle surface in the environment has been difficult.¹⁻² For example, heavy metals such as As, Cr, Cd, Pb, Hg can react with NPs through electrostatic or Van der Waals forces or form strong chemical bonds with surface exposed species³ generating surface complexes and inducing possible changes in their redox state.⁴⁻¹¹ Although there are several spectroscopic and microscopic techniques that can characterize these properties, these methods require a relatively large amount of material, they analyze only a limited number of samples and the information provided is characteristic of the bulk NPs properties. More importantly conventional methods require sample processing (filtration, drying, etc.) which can modify the NPs physicochemical characteristics. Thus, surface reactions at NP/water and NP/contaminant interface are not directly determined using conventional methods.

Single NP collision electrochemistry (SPCE)¹²⁻¹⁴ allows assessment of the physicochemical properties of single particles, as they interact and collide with an UME (Au, Pt, carbon, etc). Collision signals are obtained through indirect measurement, via an electrochemical redox probe (*e.g.* N₂H₄, H₂O₂, O₂, H₂O, BH₄), or by direct measurement, when the NP or tagged NPs (with the redox constituent immobilized onto surface) is reduced or oxidized on contact with the UME.¹⁵ The typical collision profiles of current – time (*i-t*) responses are seen as either 'staircase' or 'spike' signals and can be related with variations of size, agglomeration degree and concentration of NPs, their surface coating and the indicator redox reaction. In the last few years, the method has continuously evolved,¹⁶ with several groups making significant contributions to the fundamental understanding of electrochemical processes at single entity levels. These include: (*i*) innovations in electrode materials: Hg- or Bi- modified Pt UME,¹⁷⁻¹⁸ TiO₂/Pt UME,¹⁹ PtO_x,²⁰ boron – doped diamond UME,²¹ poly- electrolyte modified Au UME,²² (*ii*) applicability to different types of NPs: IrO_x,²³ Au,²⁴ Ni,²⁵ Cu,²⁶ fullerene,²⁷ graphene,²⁸ magnetically Prussian blue – modified Fe₃O₄ NPs,²⁹ Pd - modified carbon nanotubes,³⁰ polymer-modified Ag NPs³¹ as

well as organic NPs³² and enzymes³³ and (*iii*) reaction mechanisms including: photoelectron transfer at single TiO₂³⁴ or ZnO³⁵ NPs, characterization of the catalytic properties of nanoenzyme mimetics of Au NPs³⁶ and tracking the dynamics of individual NPs collision events.³⁷ In a previous report, we have demonstrated the use of SPCE as a rapid and cost-effective screening approach to evaluate the antioxidant activity of CeO₂ NPs.³⁸ We also reported for the first time the use of this technique for sensitive and selective detection of a toxic – ochratoxin A – by measuring the individual collision events between ssDNA aptamer-functionalized Ag NPs and a carbon fiber microelectrode.³⁹ Compared to other methods, SPCE provides several distinct advantages such as high sensitivity, elemental specificity and the possibility to quantitatively measure redox processes at single particle surfaces, including speciation. Surface adsorption of redox species on NP surfaces in aqueous dispersions can also be assessed.

Here, we evaluate the use of SPCE to investigate environmental redox reactions, speciation and surface adsorption processes occurring between a representative metal oxide NPs, cerium oxide (CeO₂), and arsenic (As), selected here as a model heavy metal co-contaminant. CeO₂ is widely used as a polishing agent in the circuit boards manufacturing and as a catalyst in catalytic convertors. 40 Therefore, a large amount of CeO2 is expected to be released in the environment, where they can react with existing contaminants.⁴¹ Arsenic is a well-known contaminant widely recognized for its public health issues. In the environment, As can be found in two oxidation states of varying toxicity, the more mobile and toxic form arsenite As3+ and its oxidized counterpart, arsenate As5+ with 10 µg/L EPA limit in drinking water. Metal oxide NPs such as CeO₂ act as sorbents of heavy metals^{4-5, 7} and can serve as a transport vector in environmental systems. Additionally, they can participate in a range of environmental redox reactions. For example, Mn-oxide(s) directly oxidizes As³⁺ to As⁵⁺ followed by surface sorption of the less toxic As⁵⁺. ⁴² The adsorption characteristics of ceria-based materials for heavy metals is in general non-specific⁴³ and applies to a variety of metal ions such as Hg and Pb⁴⁴, Cd, Pb, Cr⁴⁵, or Se, As, Cu and Pb⁴⁶⁻⁴⁷. Only a few reports investigated the adsorption of As³⁺, the most toxic form of As, by CeO₂ and related cerium-based materials.⁴⁸⁻⁵⁰ As dual oxidation state catalysts with mixed Ce³⁺/Ce⁴⁺ valence at their surface, CeO₂ NPs can participate in electron exchange reactions with As3+ ions present in solution. The chemical interactions and redox processes occurring between the surface Ce³⁺/Ce⁴⁺ and As³⁺ at the surface of individual CeO₂ and

the amount of As accumulated on single particles (single particle loading) have not been studied and are difficult to evaluate with conventional spectroscopic and microscopic methods.

While advantages of SPCE have been demonstrated, no prior work has been reported on the use of electrochemistry to examining environmental redox processes and interactions of NPs with environmental co-contaminants occurring in aqueous media. We propose in this work to use electrochemical collision signals of the NPs with a Pt UME to probe redox processes occurring at the surface of CeO₂ exposed to As³⁺. This new method monitors the interaction of heavy meals with the NPs, quantifies redox changes of the NP surface and identifies the amount and the oxidation state of heavy metal retained to each particle surface. Determining these parameters at single NPs is an important fundamental step to evaluating chemical reactions at the NP/contaminant interface in aquatic systems and developing behavior and toxicity profile of these contaminants to support more accurate environmental risk predictions.

RESULTS AND DISCUSSION

Until now, reactions of heavy metals with metal oxides have been studied by spectroscopic techniques. In this work, SPCE is proposed as a new method to investigate the interaction between CeO₂ NPs and As³⁺ and obtain a quantitative measure of the heavy metal loading on each NP. Exposure experiments were performed by traditional batch reactions with the CeO₂ NPs dispersions subjected to As³⁺ at various concentrations and different pH values. When the pH is lower than 8, As3+ exists preponderantly as H3AsO3, and when the pH is over 8, it is present as charged $H_2AsO_3^-$ (p $K_a = 9.22$). The reaction proceeds through the reactive OH groups at the CeO₂ surface, and is pH dependent. SPCE experiments were performed using a Pt-UME as working electrode and signals were used to analyze surface-bound As species. The measurements were performed in nitrogen purged solutions containing bare CeO₂ NPs and with CeO₂ NPs exposed to As³⁺ solutions of concentrations ranging from 0.1 to 100 µM. The protocol of the exposure experiments is described in detail in Supporting Information (SI) and represented schematically in Figure S1. Collision measurements were performed after 24 h incubation of CeO₂ with As³⁺ solution, when the charge passed per impact spike remained constant. Collision events were monitored in either oxidative or reductive mode, at a positive potential (0.8V vs. Ag/AgCl) when the current spikes are generated by the oxidation of As³⁺ to As⁵⁺, or at a negative

potential (-0.3V vs. Ag/AgCl) by assessing the reduction process of As³⁺ to As⁰. By measuring the charge passed per each impact and assuming that the particles are spherical and that the oxidation/reduction applies to species adsorbed on NP, As³⁺ concentration retained on the surface of each particle can be calculated.

The first set of experiments investigated the dynamic interaction between CeO₂ and As³⁺ using SPCE and cyclic voltammetry (CV). Measurements recorded as *I-t* plots detected a number of spikes for both oxidation (As³⁺/As⁵⁺) and reduction (As³⁺/As⁰) processes indicating the presence of As³⁺ onto the CeO₂ NPs surface. The process is illustrated in Figure 1 which shows the current transients generated by impacts of As³⁺- CeO₂ at pH 8 as a consequence of As³⁺/As⁵⁺ oxidation or As³⁺/As⁰ reduction. These are assigned to the oxidation (or reduction) of the surface adsorbed As, which accumulate on the NPs in solution and subsequently make contact with the working electrode by random NPs impacts. The resulting *I-t* traces thus suggest that SPCE can be used to reveal the presence and oxidation state of As species adsorbed on the surface of individual NPs, measured in the potential range corresponding to their oxido-reduction.

To confirm the identity of collision responses, CV experiments were performed at a Pt-disk electrode in a solution containing As³⁺ or drop casted CeO₂ and As³⁺-CeO₂ NPs (Figure 2). In the absence of As, the CVs of both bare Pt electrode and drop casted CeO₂ NPs onto Pt showed the electrochemical profile characteristic of Pt, with peak corresponding to surface oxide formation at potentials higher than 0.34V in the positive scan. On the reverse scan, the first peak at -0.064V is attributed to PtO reduction.⁵³⁻⁵⁴ The peak at -0.47V and those between -0.6 V and -0.3V correspond to the adsorption/desorption processes of hydrogen at Pt electrode.⁵⁵⁻⁵⁶ In the presence of As³⁺, the anodic scan shows three distinctive peaks at -0.15V, 0.44V and 0.6V respectively. The first peak is due to the oxidation of newly deposited As⁰ to As³⁺. The peak at 0.44V corresponds to the oxido/reduction of As³⁺/As⁵⁺ from As³⁺ adsorbed as As(OH)₃ electrocatalyzed by PtOH,⁵³ while the peak at 0.6 V corresponds to PtO formation.

Increasing the concentration of As induces an increase in the i_{pa1} at 0.44V in the i-E curves (Figure S2a). These results suggests an As³⁺ oxidation mechanism on oxide free surface,⁵⁴ (eq 1), followed by PtO formation through PtOH and adsorbed hydroxyl radicals (eq. 2).

$$As(OH)_3 + H_2O \rightarrow OAs(OH)_3 + 2H^+ + 2e^-$$
 (1)

$$Pt + H_2O \rightarrow PtO + 2H^+ + 2e^-$$
 (2)

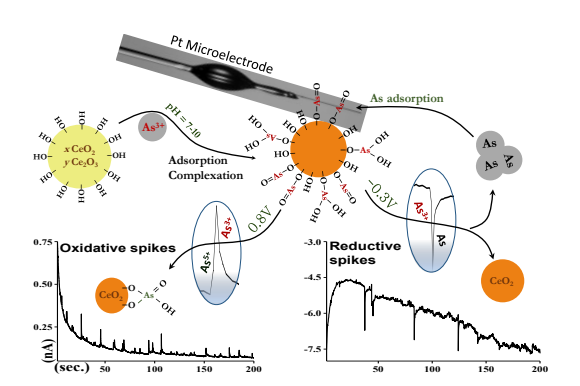


Figure 1. Schematic representation of the collision of As³⁺ adsorption on CeO₂ NPs and the resulting current transients measured in reductive (-0.3 V) and oxidative (0.8 V vs Ag/AgCl) conditions in PB at pH 8.

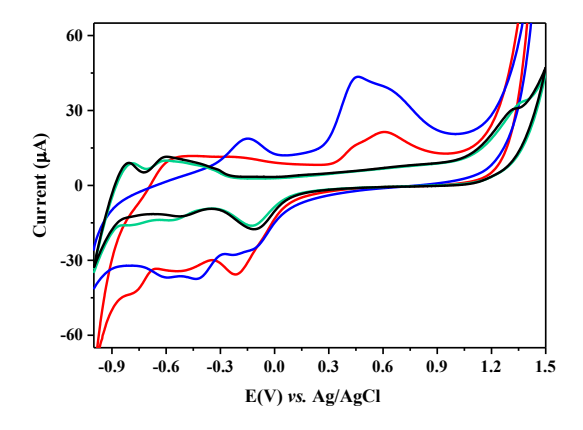


Figure 2. CVs of Pt-disk (black), CeO_2 NPs (green), $10 \mu M$ As (blue), and As^{3+} - CeO_2 NPs (red) in PB. The scan rate was 100 mV/s.

The CV of As-CeO₂ showed similar characteristics as As in solution, demonstrating that electrochemistry can be used to measure As adsorbed species onto NP surface - Figure 2(red). We further used SPCE to evaluate the effect of pH on As³⁺ adsorption. Adsorption experiments were carried out in triplicates for each pH value tested. The radius of Pt-UME electrode (*r*) calculated from the limited current value obtained from the CV carried out in FeMeOH solution (Figure S2b) was 53 μm. Control experiments in absence of As³⁺ showed few spikes, with very low current intensities below 5pA (Figure 3a) indicating no electrochemical activity of CeO₂ NPs. Note that in this work only oxidative peaks having an intensity higher than 15pA representing three times higher values than signal/noise (S/N) ratio were considered. The chronoamperograms of CeO₂ exposed to 0.1 mM As³⁺ at pHs of 4, 8 and 12 clearly show presence of current spikes due to the electrochemical oxidation of As³⁺ to As⁵⁺ that vary in

frequency and intensity with the pH (Figure 3b-d). The lowest number of spikes (5 ± 3) was recorded for the As³⁺- CeO₂ at pH 4. Significantly higher number of spikes were observed for pH 8 (17 \pm 4) and pH 12 (21 \pm 7). Theoretically, since the NPs concentration is the same, the number of current spikes is expected to be relatively the same. However, at pH 4, the number of spikes is lower due to the presence of stable uncharged H₃AsO₃ and therefore a lower amount of adsorbed As (or under the detection limit). The average current at pH 4 was ~ 23 pA, while at pH 8 and 12 the current intensity increased to ~95 pA and ~98 pA respectively. The UV-Vis spectrum of CeO₂ at pH 8 shows a peak associated to Ce⁴⁺ at ~303 nm. At pH 4, the Ce⁴⁺ peak is present at ~346 nm⁵⁷ (Figure S3), suggesting possible agglomeration of the NPs in acidic media. When CeO₂ was treated with As³⁺ at pH 4, the Ce⁴⁺ peak shifted to 330 nm. In this case, physisorption of H₃AsO₃ stabilizes the NPs dispersion. Possible oxidation of As³⁺ to As⁵⁺ by surface Ce⁴⁺ ions may also occur, as previously suggested by Everett and Skoog.⁵⁸ In this case, the interaction of CeO₂ NPs with As³⁺ can be a combination of oxidation and sorption similar to that reported for MnO₂.⁴² Therefore, the NP surface may contain As³⁺ and the newly formed As⁵⁺ stabilized through hydroxyl groups as monodentate (As³⁺, As⁵⁺) or bidentate (As⁵⁺) complexes.⁵⁹ When these processes were studied by SPCE at this pH value, the particles exposed to As³⁺ showed the lowest number of oxidative spikes with the lowest current intensity. This indicates a low concentration of As species adsorbed onto CeO₂ NPs, possibly due to a low conversion rate of As3+ to As5+ and the lack of interaction between the protonated surface of CeO2 and H3AsO3. These finding are in line with prior works reporting low removal efficiency of As³⁺ by CeO₂ in acidic pH (<4).⁷ At pH 8, the peak of Ce⁴⁺ in the UV-Vis spectra shifts slightly from 303 to 313 nm in the As-treated sample, due to As adsorption. At pH 12, the presence of As induced a decrease in the Ce⁴⁺ peak and a shift from 303 to 312 nm due to NPs agglomeration (Figure S3).

Full width at half maximum (FWHM) of peaks for CeO_2 NPs exposed to As^{3+} at pH 4 and 8 ranged between 0.11 and 0.13 sec. The FWHM of peaks at pH 12 (Figure 3) was ~ 0.25 sec or 0.32 sec suggesting collisions with agglomerated particles. The deconvolution of peaks (Origin 9.0 software) associated with those collisions (Figure 3d right) indicates collisions with aggregates of 2 - 3 NPs. This finding is supported by DLS measurements of the particles exposed to As^{3+} showing an increase in the particle size from ~ 90 -110 nm at pH 4 to ~ 230 nm at pH 12. The average charge per impact transient calculated from few hundred spikes of As-exposed CeO_2 was: 0.63×10^{-12} C, 2.93×10^{-12} C and 9.75×10^{-12} C at pH 4, 8 and 12 respectively (Figure

S4). By taking into account the charge and the number of electrons involved in *eq*. 3, the average numbers of As atoms attached onto single CeO₂ NP can be found.¹⁵

$$Q = n e N_{As}$$
 (3)

(where: n=2, $e = 1.6 \times 10^{-19}$ C and N_{As} - the number of As atoms)

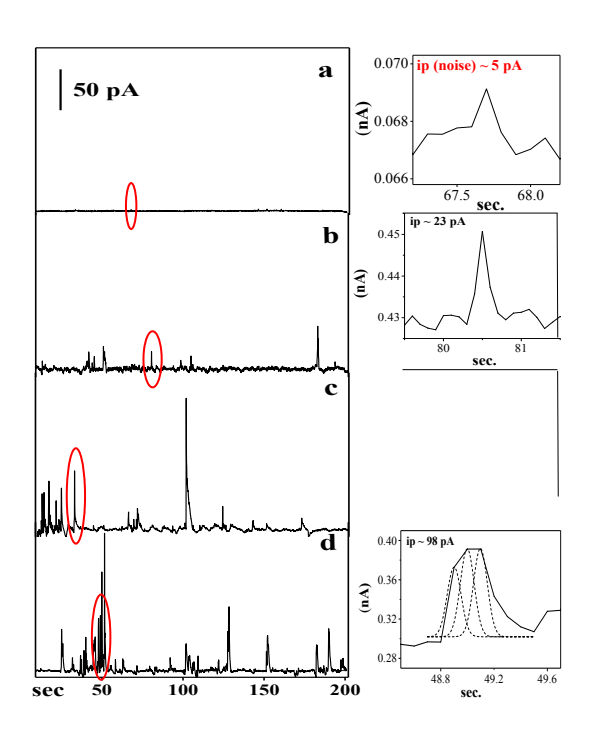


Figure 3. *I-t* profile recorded at 0.8V of CeO_2 (a) and CeO_2 NPs exposed to As^{3+} (0.1 mM) at pH 4 (b), pH 8 (c) and pH 12 (d) with zoom on representative current transients (right).

Table S1 shows the physicochemical characteristics of CeO₂ exposed to As³⁺ at pH 4, 8 and 12 respectively. For NPs exposed to As at pH 4 about 22% of the surface is occupied by As, while for NPs exposed at a pH higher than 8 nearly the entire surface is covered by adsorbed As. The high loading of As³⁺ on CeO₂ in basic conditions calculated from charge measurements suggests that adsorption in basic media is significantly higher than in acidic media. These results are in good agreement with the previous studies of As³⁺ adsorption on ceria.^{15, 48} Since uncharged H₃AsO₃ is the dominant species in acidic or neutral aqueous solutions, adsorption on solid materials is limited. At pH 4, the CeO₂ NPs are positively charged (+36.92±5.44 mV) and have little attractive effect on H₃AsO₃.⁴⁸ At low pH, the Ce⁴⁺ with a high standard reduction potential (Ce⁴⁺/Ce³⁺ = 1.61V) and can oxidize As³⁺ to As⁵⁺ (As⁵⁺/As³⁺ = 0.56V). In this case, the redox process involving the Ce³⁺/Ce⁴⁺ species and the size (surface area) of CeO₂ are expected to

be the dominant factors. At pH 8, the zeta potential of CeO₂ measured in PB solution was -30.63 ± 4.35 mV. Under weakly alkaline conditions (pH 8-10), adsorption is expected through the highly hydroxylated species of the CeO₂ surface. Prior studies of As³⁺ removal by CeO₂-based oxides, $^{48-49, 52, 59}$ showed a maximum As³⁺ adsorption under alkaline conditions. A strong affinity between H₂AsO₃⁻ anions and CeO₂ is expected. This interaction involves a hydrated Ce⁴⁺ form, Ce(H₂O)_x(OH)_y(4-y)+ which is further stabilized by counter ions. $^{57, 60-61}$ The H₂AsO₃⁻ which is the most dominating species at a pH>8 can stabilize the hydrated Ce⁴⁺ complex. This interaction could explain the highest As removal efficiency observed previously in the pH range of 8-10. $^{48-49, 51-52, 59}$

To further confirm the composition and the Ce, As and O valence states and validate the collision data, the surface of NPs before and after As adsorption were studied by XPS. The Ce3d spectra (Figure S5) confirms the presence of both 4+ and 3+ valence states of cerium at the CeO₂ surface. The concentration of Ce³⁺ calculated from the corresponding area peaks⁶² assigned to Ce³⁺ and Ce⁴⁺ before As adsorption was 23.6, 24.8 and 22.8% for pH 4, 8 and 12 respectively. After As adsorption, the Ce³⁺ content increased to 27.7% for adsorption at pH 4, while for the other two pH values the Ce³⁺ content remained nearly the same, 24.1% at pH 8 and 22.8% at pH 12. The high resolution O1s spectra before and after As adsorption, as well as the As3d spectra of CeO₂ NPs at the three pH values tested are illustrated in Figure 4. The O1s spectrum of bare CeO₂ at pH 4 can be deconvoluted into three overlapped peaks (Figure 4a). The first on at 529.8 eV corresponds to lattice oxygen as Ce⁴⁺-O, the one at 531 eV is associated with the oxygen atoms in Ce³⁺-O,⁶³ while the peak at 531.5 eV can be attributed to the surface bond hydroxyl groups (Ce-OH).⁶⁴ After As adsorption, the O1s spectrum shown an additional peak at 533.2 eV associated to the surface adsorbed water molecules (Figure 4d). The As spectrum has two fitted peaks associated with As³⁺-O at 44 eV and As⁵⁺-O at 45.4 eV (Figure 4g).⁶⁵ The presence of As⁵⁺-O peak concurrently with the increase in the ratio of oxygen bound to Ce³⁺ from 10% to 29% after As adsorption, suggests partial oxidation of As³⁺ to As⁵⁺ during the adsorption process at this pH value (pH 4). A similar trend was reported previously for the adsorption of As onto Ce-Fe mixed oxide⁶⁵ or CeO₂-graphene oxide.⁶⁶ The O1s spectra of the CeO₂ NPs dispersed in solutions with pH of 8 or 12 before exposure to As show characteristic features of Ce-O (~ 530 eV), Ce-OH (~531.4 eV) and adsorbed water (~533 eV) – Figures 4b,c. After As adsorption, a new peak ~ 527 eV appeared in the O1s XPS spectra, assigned to As-O bond (Figures 4e,f).⁶⁷

The corresponding area of this peak decreases from 12% for the As-exposed CeO_2 at pH 8 to \sim 8% as compared to those at pH 12 proving that slight basic condition are more favorable for As adsorption. The XPS spectra of As3d for the NPs exposed to As at pH 8 and 10 has two components (43.6 – 44.6 eV) associated with As-O and As_2O_3 (Figures 4h,i).⁶⁸ The absence of the As^{5+} peak at \sim 45.5 eV suggests no As^{3+} oxidation process for these basic pH values. The XPS results are in good agreement and confirm the electrochemical collision data, demonstrating that collision can be used as an alternative method to identify adsorption processes and speciation of heavy metal adsorption at NPs surfaces. Further electrochemical studies to assess the effect of NP and As concentrations were performed at pH 8.

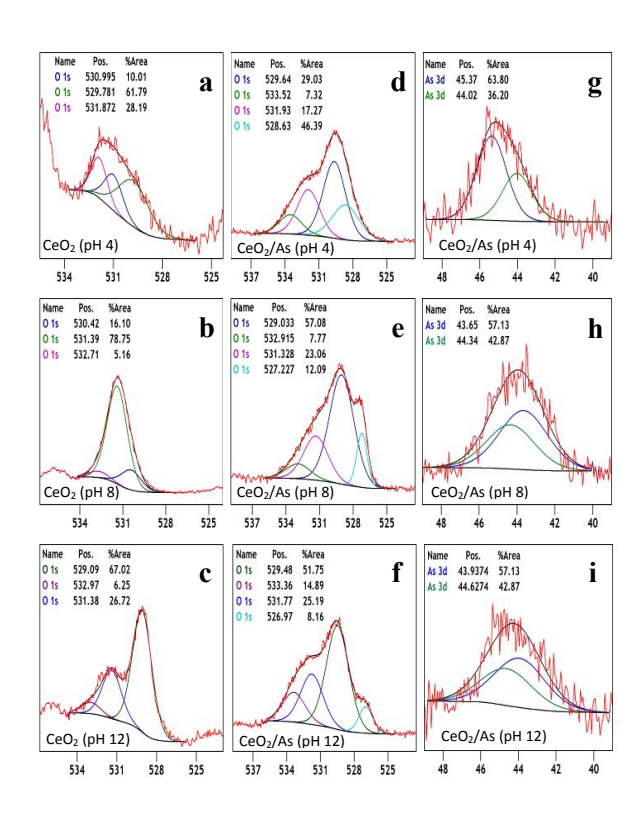


Figure 4. The O1s XPS spectra (a,b,c) of CeO₂ and the O1s (d,e,f) and As3d (g,h,i) XPS spectra of the NPs exposed to As at different pH values: 4, 8 and 12 respectively.

The As-CeO₂ concentration showed a linear increase in number of spikes in both anodic and or cathodic regions with increasing the particle concentration (Figure 5). However, several differences are seen between the anodic and cathodic regimes. First, the reductive current transients recorded at -0.3V with bare CeO₂ (Figure S6), are higher (~ 20 pA), than the residual current (~ 5 pA) in the oxidative regime. This is due to the influence of oxygen reduction reaction

(ORR) and possibly the hydrogen evolution at Pt UME occurring at a potential lower than -0.3V. In this case, current transients with intensities higher than 50pA were considered in data analysis. The chronoamperometric profile recorded under reductive conditions contained a combination of both "spike" and "staircase" signals. The latter is attributed to the accumulation of As⁰ onto the Pt-ME surface, a process that occurs when the NPs-carrying As collide and transfer the adsorbed As to the Pt-ME.¹³ Indeed, the linear sweep voltammetry (LSV) between 0 and 1V with a Pt-ME before and after use in a reductive collision measurement showed a well-defined oxidative peak at 0.7V representing the stripping of the As accumulated onto the Pt-ME surface during the collision experiment (Figure S7).

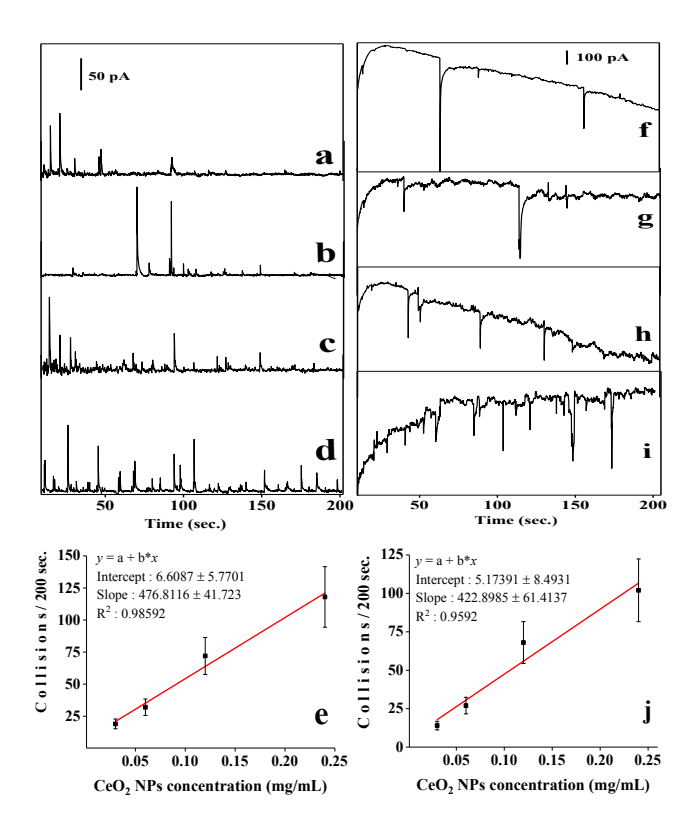


Figure 5. *I-t* profile recorded at 0.8 V (a-d) and -0.3 V (f-i) of CeO₂ exposed to As³⁺ at pH 8 at different NP concentrations: 0.03 (a,f), 0.06 (b,g), 0.12 (c,h) and 0.24 mg/mL (d,i) with the correspondent concentration-collisions dependency curves for oxidative spikes (e) and reductive spikes (j) respectively. The error bars represent the standard deviation of five replicates.

A comparison between the experimental and calculated frequency values of the oxidative collision events as a function of the As-CeO₂ NPs concentration (details in SI) is illustrated in Figure S8. The theoretical values are higher than experimental ones and this finding is in agreement with the previous theoretical and experimental studies.⁶⁹ This discrepancy was

associated with the NPs aggregation / precipitation / wall sticking, undetectable collisions, small untraceable transient currents⁷⁰ and in this case a possible inhomogeneous As adsorption onto the NP surface.

In a final set of experiments, we assessed if changes in the total calculated charge from collisions and/or peak collisions current intensity can be used to quantify the initial concentration of As³⁺ in solution. For measurements carried out in the negative potential range (e.g. reduction of As³⁺) where the collision process has both spikes and stairs, it is very difficult to calculate the total charge. Moreover, the presence of possible heavy metals co-contaminants (e.g. Cr^{6+}/Cr^{3+} = -0.12V, $Pb^{2+}/Pb^0 = -0.13V$, $Cd^{2+}/Cd^0 = -0.40V$) may impact the selectivity of measurements. Due to these impediments, the As content in initial solutions was determined only through oxidative collisions at 0.8V. NPs exposed to a solution containing 0.1 μ M As³⁺ generated ~7 (±) 3 spikes during 200 s time measurement, while for those exposed to 1, 10 and 100 µM the number of spiked were $10(\pm 5)$, $11(\pm 5)$ and 13 ± 3 respectively - Figure 6(a-d). SPCE experiments were carried out using at least two different batches of As-CeO₂ NPs and two different electrodes. A minimum of five collision tests were run for each As concentration tested. Figures 6e and 6g show the calibration curves of total charge (Q_t) and peak current intensities (i_{pq}) vs As concentration. The average charge recorded in 200 sec for CeO₂ exposed to 0.1 µM As was 13.4 \pm 4.2 pC. The charge increased to 131 \pm 21.2 pC when the NPs were exposed to 100 μ M As. The corresponding average collision peaks current increased from ~ 28 pA to ~230 pA. A linear correlation between charge or current intensity and As3+ concentration in the exposure solution was found between 0.1 and 10 µM (Figures 6f and 6h). The error bars represent the number of five replicates. The limit of detection (C_{LOD}) was calculated using $C_{LOD} = 3s_{\nu/x} \div b$, where $s_{\nu/x}$ is the standard error of the regression and b is the slope. When the Q_t analysis was considered, the C_{LOD} was 0.65 μ M (~ 48 ppb), while for i_{pq} calibration, the C_{LOD} was 1.14 μ M (~ 85.5 ppb) respectively. This dependency can be used to determine the amount of As³⁺ in aqueous samples. The LODs obtained by SPCE falls within the range of (0.008 – 200 ppb) that was reported previously using electrochemistry.⁷¹ However, SPCE analysis reflects the amount of As³⁺ adsorbed onto NP surfaces rather than the dissolved As³⁺ previously measured by voltammetric techniques. To demonstrate this applicability water samples from a local river (Raquette River) spiked with 1 µM As³⁺ were exposed to CeO₂ NPs for 24 hrs and then the collision was recorded. The recorded chronoamperogram showed ~11 collisions with an average peak intensity of ~50

pA and average charge of 18.9 pC (Figure S9). These values are comparable with the 1 μ M As³⁺ standard solution of 57 pA and 26.1 pC respectively. These results demonstrate the potential of this method as an analytical tool to quantitatively measure the amount of As³⁺ in aqueous environments.

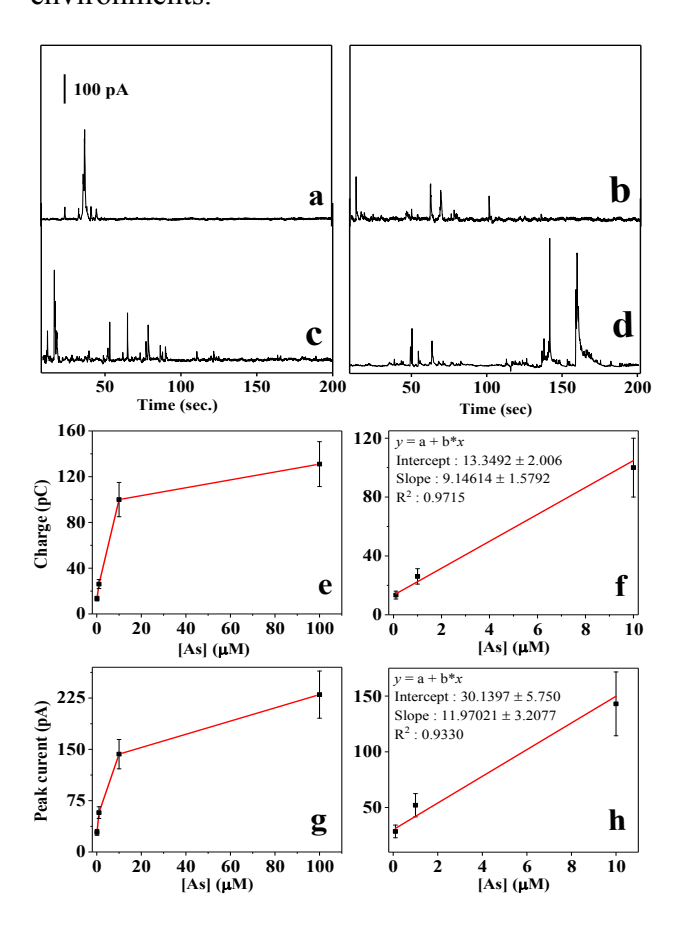


Figure 6 *I-t* profiles recorded for 200 seconds at 0.8 V (a-d) and their correspondent calibration curves of total charge (e) and current intensity (g) for CeO₂ NPs exposed to different As³⁺ concentrations: 0.1 μ M (a), 1 μ M (b), 10 μ M (c) and 100 μ M (d). Linear range of Q_t (f) an i_{pa} (h) vs As³⁺ concentration. The error bars represent the standard deviation of five replicates.

CONCLUSION

In conclusion, we demonstrated the applicability of SPCE to study the interaction, redox transformation and speciation of a representative heavy metal contaminant, As³⁺ on metal oxide NPs, using CeO₂ as a model example. The adsorption of As³⁺ and its interaction with CeO₂ NPs have been detected electrochemically either through the direct oxidation of the As³⁺ adsorbed

onto the NP surface, or reduction of As³⁺, at their corresponding potentials. We found that changes in total recorded charge and peak intensity can be used to estimate the oxidation state and the amount of As adsorbed onto each NP surface, illustrating the possibility of this method for assessing the sorption behavior and measure the local contaminant concentration and their oxidation states (loading on each particle) in different exposure conditions. The highest number of spikes was observed for As³⁺ adsorption at pH 8 suggesting a maximum adsorption capacity at this pH value. Surface adsorption of As3+ was common in basic conditions, confirming strong adsorption onto CeO₂ NPs. In acidic environments (pH<4), a small fraction of As³⁺ was oxidized to As⁵⁺ by surface Ce⁴⁺ and further adsorbed onto the CeO₂ surface as a bidentate complex. The measured charge and peak current intensity can be correlated with the As3+ concentration accumulated onto the NPs, which is representative of the As concentration in solution. No other method can provide measurement of localized concentrations and speciation of environmental toxicants directly on the particle surface. A linearity between the spike frequency and As concentration was observed in the range 0.1-10 µM, indicating that the method can also be used as an analytical tool for measurements of As. A key feature of this strategy is that, unlike spectroscopic approaches, the SPCE can be used to investigate both redox and surface sorption processes occurring at the contaminant/NP interface in aqueous solutions, without any treatment of the sample, which is critical to furthering our understanding of the kinetics and reaction mechanisms of environmentally released NPs. Given the elemental speciation and high sensitivity of the method, single particle electrochemistry has many potential applications for material characterization and fundamental studies of redox reactions occurring in aqueous media at resolution scales unattainable by currently used methods.

MATERIALS AND METHODS

Reagents. Cerium (IV) oxide nanopowder (10-20 nm) (Catalog # 544841) was purchased from Sigma Aldrich. As₂O₃ was purchased from J.T. Baker. PFA-Coated Platinum Wire (Catalog: 771000), $\phi = 50.8$ μm was purchased from A-M systems. Silver conductive epoxy was obtained from MG Chemicals. Non-conductive epoxy was purchased from Devcon. Ferrocenemethanol 97% (FeMeOH) and Na₂SO₄ were purchased from Sigma Aldrich. DI water (Millipore, Direct-Q System) with a resistivity of 18.2Ω cm was used for preparation of solutions. For buffer solution, 0.1 M phosphate buffer (PB) was made from sodium phosphate (monobasic and dibasic) (Fisher

Sci.) and adjusted to pH 8. The As³⁺ stock solution (2 mg/ml) was prepared by dissolving arsenic trioxide in 0.1 M NaOH (Fisher Sci.).

Instrumentation. Electrochemical experiments were performed using a CHI800 (CH Instruments Inc.). All electrochemical experiments were carried out using a conventional three electrodes electrochemical cell with a Pt-UME as the working electrode, Ag/AgCl as reference electrode and a platinum wire as counter electrode. All potentials were referred to the Ag/AgCl reference electrode. The UV studies were performed with a Shimadzu PC-2401 spectrophotometer using 1 cm quartz cell. The particles size distribution and the zeta potential were measured with a Brookhaven Zeta Pals analyzer. The XPS measurements were performed at Cornell Center for Materials Research (CCMR) using a Surface Science Instruments SSX-100 with operating pressure ~2x10-9 Torr. Monochromatic Al K_{α} X-ray (1486.6 eV) with 1 mm diameter beam size was used. Photoelectrons were collected at a 55° emission angle. A hemispherical analyzer determined electron kinetic energy, using pass energy of 150V for wide/survey scans, and 50V for high resolution scans. A flood gun was used for charge neutralization of non-conductive samples.

UV-Vis Spectroscopy Experiments. Ceria (CeO₂) NPs were dispersed in solution with different pH values of 4, 8, 12 (HCl and NaOH were used to regulate pH) with the final concentration of 0.05 mg/ml. For exposure studies, the CeO₂NPs were dispersed in solutions of As of different pH values (4, 8, 12) and incubated for 24 h before analysis.

Real Sample Measurements. Applicability of the collision protocol to measure As content in real samples was demonstrated using water collected from Raquette River in Potsdam, NY, USA. In order to remove any solids impurities, the river water was filtered using a Whatman filter paper. Then, CeO_2 NPs (0.25 mg/ml) was added and the water was spiked with As^{3+} solution (1 μ M) and incubated at RT for 24 h. After centrifugation (10,000 rpm for 5 min), the supernatant was removed and the particles were washed twice with DI. The exposed NPs were dispersed in 4 ml electrochemical cell and measured by single particle collision electrochemistry. Figure S7 shows collision profiles for real sample analysis using river water spiked with 1 μ M As³⁺ and exposed to CeO_2 for 24 hrs.

ASSOCIATED CONTENT

Supporting Information.

Electrochemical measurements and preparation of Pt-UME. UV-Vis measurements of bare CeO_2 and As-exposed CeO_2 NPs. The charge distribution per impact transient of As-exposed CeO_2 . Physicochemical characteristics of CeO_2 NPs exposed to As^{3+} at different pH values. The Ce3d XPS spectra of bare and As-exposed CeO_2 NPs at different pH values. Linear sweep voltammetry (LSV) of a Pt-UME before and after use in an electrochemical reductive collision experiment. Chronoamperometric measurement of CeO_2 NPs exposed to 1 μ M As solution spiked in a river water sample.

AUTHOR INFORMATION

Corresponding Author *E-mail: eandrees@clarkson.edu

Author Contributions: the manuscript was written through contributions of all authors. All authors have given approval to the final version of the manuscript.

Notes: the authors declare no competing financial interest.

ACKNOWLEDEGMENTS

This material is based upon work supported by the National Science Foundation (NSF) under Grant 1610281. Any opinions, findings, and conclusions or recommendations expressed in this material are those of the author(s) and do not necessarily reflect the views of the NSF.

REFERENCES

- (1) Preda, G.; Migani, A.; Neyman, K. M.; Bromley, S. T.; Illas, F.; Pacchioni, G. Formation of Superoxide Anions on Ceria Nanoparticles by Interaction of Molecular Oxygen with Ce3+ Sites. *J. Phys. Chem. C* **2011**, *115*, 5817-5822.
- (2) Whitley, A. R.; Levard, C.; Oostveen, E.; Bertsch, P. M.; Matocha, C. J.; von der Kammer, F.; Unrine, J. M. Behavior of Ag Nanoparticles in Soil: Effects of Particle Surface Coating, Aging and Sewage Sludge Amendment. *Environ. Pollut.* **2013**, *182*, 141-149.
- (3) Hayes, S. A.; Yu, P.; O'Keefe, T. J.; O'Keefe, M. J.; Stoffer, J. O. The Phase Stability of Cerium Species in Aqueous Systems I. E-pH Diagram for the Ce-HClO₄-H₂O System. *J. Electrochem. Soc.* **2002**, *149*, C623-C630.
- (4) Peng, X. J.; Luan, Z. K.; Ding, J.; Di, Z. H.; Li, Y. H.; Tian, B. H. Ceria Nanoparticles Supported on Carbon Nanotubes for the Removal of Arsenate from Water. *Mater. Lett.* **2005**, *59*, 399-403.

- (5) Di, Z. C.; Ding, J.; Peng, X. J.; Li, Y. H.; Luan, Z. K.; Liang, J. Chromium Adsorption by Aligned Carbon Nanotubes Supported Ceria Nanoparticles. *Chemosphere* **2006**, *62*, 861-865.
- (6) Li, R. H.; Li, Q.; Gao, S.; Shang, J. K. Exceptional Arsenic Adsorption Performance of Hydrous Cerium Oxide Nanoparticles: Part A. Adsorption Capacity and Mechanism. *Chem. Eng. J.* **2012**, *185*, 127-135.
- (7) Feng, Q. Z.; Zhang, Z. Y.; Ma, Y. H.; He, X.; Zhao, Y. L.; Chai, Z. F. Adsorption and Desorption Characteristics of Arsenic onto Ceria Nanoparticles. *Nanoscale Res. Lett.* **2012**, *7*, 1-8.
- (8) Ozel, R. E.; Alkasir, R. S. J.; Ray, K.; Wallace, K. N.; Andreescu, S. Comparative Evaluation of Intestinal Nitric Oxide in Embryonic Zebrafish Exposed to Metal Oxide Nanoparticles. *Small* **2013**, *9*, 4250-4261.
- (9) Collin, B.; Oostveen, E.; Tsyusko, O. V.; Unrine, J. M. Influence of Natural Organic Matter and Surface Charge on the Toxicity and Bioaccumulation of Functionalized Ceria Nanoparticles in Caenorhabditis elegans. *Environ. Sci. Technol.* **2014**, *48*, 1280-1289.
- (10) Ginder-Vogel, M.; Landrot, G.; Fischel, J. S.; Sparks, D. L. Quantification of Rapid Environmental Redox Processes with Quick-scanning X-ray Absorption Spectroscopy (Q-XAS). *P. Natl. Acad. Sci. USA* **2009**, *106*, 16124-16128.
- (11) Wagner, S.; Gondikas, A.; Neubauer, E.; Hofmann, T.; von der Kammer, F. Spot the Difference: Engineered and Natural Nanoparticles in the Environment—Release, Behavior, and Fate. *Angew. Chem. Int. Ed.* **2014**, *53*, 12398-12419.
- (12) Xiao, X.; Bard, A. J. Observing Single Nanoparticle Collisions at an Ultramicroelectrode by Electrocatalytic Amplification. *J. Am. Chem. Soc.* **2007**, *129*, 9610-9612.
- (13) Xiao, X.; Fan, F.-R. F.; Zhou, J.; Bard, A. J. Current Transients in Single Nanoparticle Collision Events. *J. Am. Chem. Soc.* **2008**, *130*, 16669-16677.
- (14) Andreescu, D.; Kirk, K. A.; Narouei, F. H.; Andreescu, S. Electroanalytic Aspects of Single-Entity Collision Methods for Bioanalytical and Environmental Applications. *Chemelectrochem* **2018**, *5*, 2920-2936.
- (15) Zhou, Y. G.; Rees, N. V.; Compton, R. G. The Electrochemical Detection of Tagged Nanoparticles via Particle-Electrode Collisions: Nanoelectroanalysis Beyond Immobilisation. *Chem. Commun.* **2012**, *48*, 2510-2512.
- (16) Cheng, W.; Compton, R. G. Electrochemical detection of nanoparticles by 'nano-impact' methods. *Trac-Trend Anal. Chem.* **2014**, *58*, 79-89.
- (17) Dasari, R.; Walther, B.; Robinson, D. A.; Stevenson, K. J. Influence of the Redox Indicator Reaction on Single-Nanoparticle Collisions at Mercury- and Bismuth-Modified Pt Ultramicroelectrodes. *Langmuir* **2013**, *29*, 15100-15106.
- (18) Dasari, R.; Tai, K.; Robinson, D. A.; Stevenson, K. J. Electrochemical Monitoring of Single Nanoparticle Collisions at Mercury-Modified Platinum Ultramicroelectrodes. *ACS Nano* **2014**, *8*, 4539-4546.
- (19) Kim, J.; Kim, B.-K.; Cho, S. K.; Bard, A. J. Tunneling Ultramicroelectrode: Nanoelectrodes and Nanoparticle Collisions. *J. Am. Chem. Soc.* **2014**, *136*, 8173-8176.
- (20) Zhou, H.; Fan, F.-R. F.; Bard, A. J. Observation of Discrete Au Nanoparticle Collisions by Electrocatalytic Amplification Using Pt Ultramicroelectrode Surface Modification. *J. Phys. Chem. Lett.* **2010**, *1*, 2671-2674.
- (21) Wakerley, D.; Guell, A. G.; Hutton, L. A.; Miller, T. S.; Bard, A. J.; Macpherson, J. V. Boron Doped Diamond Ultramicroelectrodes: a Generic Platform for Sensing Single Nanoparticle Electrocatalytic Collisions. *Chem. Commun.* **2013**, *49*, 5657-5659.
- (22) Castañeda, A. D.; Alligrant, T. M.; Loussaert, J. A.; Crooks, R. M. Electrocatalytic Amplification of Nanoparticle Collisions at Electrodes Modified with Polyelectrolyte Multilayer Films. *Langmuir* **2015**, *31*, 876-885.
- (23) Kwon, S. J.; Fan, F.-R. F.; Bard, A. J. Observing Iridium Oxide (IrOx) Single Nanoparticle Collisions at Ultramicroelectrodes. *J. Am. Chem. Soc.* **2010**, *132*, 13165-13167.

- (24) Zhou, Y. G.; Rees, N. V.; Pillay, J.; Tshikhudo, R.; Vilakazi, S.; Compton, R. G. Gold Nanoparticles Show Electroactivity: Counting and Sorting Nanoparticles Upon Impact with Electrodes. *Chem. Commun.* **2012**, *48*, 224-226.
- (25) Stuart, E. J. E.; Zhou, Y. G.; Rees, N. V.; Compton, R. G. Determining Unknown Concentrations of Nanoparticles: the Particle-Impact Electrochemistry of Nickel and Silver. *RCS Adv.* **2012**, *2*, 6879-6884.
- (26) Haddou, B.; Rees, N. V.; Compton, R. G. Nanoparticle-Electrode Impacts: the Oxidation of Copper Nanoparticles has Slow Kinetics. *Phys. Chem. Chem. Phys.* **2012**, *14*, 13612-13617.
- (27) Stuart, E. J. E.; Tschulik, K.; Batchelor-McAuley, C.; Compton, R. G. Electrochemical Observation of Single Collision Events: Fullerene Nanoparticles. *ACS Nano* **2014**, *8*, 7648-7654.
- (28) Li, D.; Liu, J. Q.; Barrow, C. J.; Yang, W. R. Protein Electrochemistry Using Graphene-Based Nano-assembly: an Ultrasensitive Electrochemical Detection of Protein Molecules via Nanoparticle-Electrode Collisions. *Chem. Commun.* **2014**, *50*, 8197-8200.
- (29) Santos, G. P.; Melo, A. F. A. A.; Crespilho, F. N. Magnetically Controlled Single-Nanoparticle Detection via Particle-Electrode Collisions. *Phys. Chem. Chem. Phys.* **2014**, *16*, 8012-8018.
- (30) Hodson, H.; Li, X.; Batchelor-McAuley, C.; Shao, L.; Compton, R. G. Single Nanotube Voltammetry: Current Fluctuations Are Due to Physical Motion of the Nanotube. *J. Phys. Chem. C* **2016**, *120*, 6281-6286.
- (31) Karimi, A.; Kirk, K. A.; Andreescu, S. Electrochemical Investigation of pH-Dependent Activity of Polyethylenimine-Capped Silver Nanoparticles. *Chemelectrochem* **2017**, *4*, 2801-2806.
- (32) Cheng, W.; Zhou, X. F.; Compton, R. G. Electrochemical Sizing of Organic Nanoparticles. *Angew Chem Int Edit* **2013**, *52*, 12980-12982.
- (33) Sekretaryova, A. N.; Vagin, M. Y.; Turner, A. P. F.; Eriksson, M. Electrocatalytic Currents from Single Enzyme Molecules. *J. Am. Chem. Soc.* **2016**, *138*, 2504-2507.
- (34) Peng, Y.-Y.; Ma, H.; Ma, W.; Long, Y.-T.; Tian, H. Single-Nanoparticle Photoelectrochemistry at a Nanoparticulate TiO2-Filmed Ultramicroelectrode. *Angew. Chem. Int. Ed.* **2018**, *57*, 3758-3762.
- (35) Ma, H.; Ma, W.; Chen, J.-F.; Liu, X.-Y.; Peng, Y.-Y.; Yang, Z.-Y.; Tian, H.; Long, Y.-T. Quantifying Visible-Light-Induced Electron Transfer Properties of Single Dye-Sensitized ZnO Entity for Water Splitting. *J. Am. Chem. Soc.* **2018**, *140*, 5272-5279.
- (36) Hafez, M. E.; Ma, H.; Ma, W.; Long, Y.-T. Unveiling the Intrinsic Catalytic Activities of Single-Gold-Nanoparticle-Based Enzyme Mimetics. *Angew. Chem. Int. Ed.* **2019**, *131*, 6393-6398.
- (37) Ma, W.; Ma, H.; Chen, J.-F.; Peng, Y.-Y.; Yang, Z.-Y.; Wang, H.-F.; Ying, Y.-L.; Tian, H.; Long, Y.-T. Tracking Motion Trajectories of Individual Nanoparticles Using Time-Resolved Current Traces. *Chem. Sci.* **2017**, *8*, 1854-1861.
- (38) Sardesai, N. P.; Andreescu, D.; Andreescu, S. Electroanalytical Evaluation of Antioxidant Activity of Cerium Oxide Nanoparticles by Nanoparticle Collisions at Microelectrodes. *J. Am. Chem. Soc.* **2013**, *135*, 16770-16773.
- (39) Karimi, A.; Hayat, A.; Andreescu, S. Biomolecular Detection at ssDNA-Conjugated Nanoparticles by Nano-impact Electrochemistry. *Biosens. Bioelectron.* **2017**, *87*, 501-507.
- (40) Dumitrescu, E.; Karunaratne, D. P.; Babu, S. V.; Wallace, K. N.; Andreescu, S. Interaction, Transformation and Toxicity Assessment of Particles and Additives Used in the Semiconducting Industry. *Chemosphere* **2018**, *192*, 178-185.
- (41) Andreescu, D.; Bulbul, G.; Ozel, R. E.; Hayat, A.; Sardesai, N.; Andreescu, S. Applications and Implications of Nanoceria Reactivity: Measurement Tools and Environmental Impact. *Environ-Sci Nano* **2014**, *1*, 445-458.
- (42) Lafferty, B. J.; Ginder-Vogel, M.; Sparks, D. L. Arsenite Oxidation by a Poorly-Crystalline Manganese Oxide. 3. Arsenic and Manganese Desorption. *Environ. Sci. Technol.* **2011**, *45*, 9218-9223.

- (43) Olivera, S.; Chaitra, K.; Venkatesh, K.; Muralidhara, H. B.; Inamuddin; Asiri, A. M.; Ahamed, M. I. Cerium Dioxide and Composites for the Removal of Toxic Metal Ions. *Environ. Chem. Lett.* **2018**, *16*, 1233-1246.
- (44) Sharma, R.; Raghav, S.; Nair, M.; Kumar, D. Kinetics and Adsorption Studies of Mercury and Lead by Ceria Nanoparticles Entrapped in Tamarind Powder. *ACS Omega* **2018**, *3*, 14606-14619.
- (45) Contreras, A. R.; Casals, E.; Puntes, V.; Komilis, D.; Sanchez, A.; Font, X. Use of Cerium Oxide (CeO2) Nanoparticles for the Adsorption of Dissolved Cadmium (Ii), Lead (Ii) and Chromium (Vi) at Two Different Phs in Single and Multi-Component Systems. *Global Nest J.* **2015**, *17*, 536-543.
- (46) Cao, C. Y.; Cui, Z. M.; Chen, C. Q.; Song, W. G.; Cai, W. Ceria Hollow Nanospheres Produced by a Template-Free Microwave-Assisted Hydrothermal Method for Heavy Metal Ion Removal and Catalysis. *J. Phys. Chem. C* **2010**, *114*, 9865-9870.
- (47) Baranik, A.; Gagor, A.; Queralt, I.; Margui, E.; Sitko, R.; Zawisza, B. Ceria Nanoparticles Deposited on Graphene Nanosheets for Adsorption of Copper(II) and Lead(II) Ions and of Anionic Species of Arsenic and Selenium. *Microchim. Acta* **2018**, *185*.
- (48) Feng, Q.; Zhang, Z.; Ma, Y.; He, X.; Zhao, Y.; Chai, Z. Adsorption and Desorption Characteristics of Arsenic onto Ceria Nanoparticles. *Nanoscale Res Lett* **2012**, *7*, 84.
- (49) Li, R.; Li, Q.; Gao, S.; Shang, J. K. Exceptional Arsenic Adsorption Performance of Hydrous Cerium Oxide Nanoparticles: Part A. Adsorption Capacity and Mechanism. *Chem. Eng. J.* **2012**, *185-186*, 127-135.
- (50) Peng, X.; Luan, Z.; Ding, J.; Di, Z.; Li, Y.; Tian, B. Ceria Nanoparticles Supported on Carbon Nanotubes for the Removal of Arsenate from Water. *Mater. Lett.* **2005**, *59*, 399-403.
- (51) Singh, D. B.; Prasad, G.; Rupainwar, D. C.; Singh, V. N. As(III) Removal from Aqueous-Solution by Adsorption. *Water Air Soil Poll.* **1988**, *42*, 373-386.
- (52) Xu, W. H.; Wang, J.; Wang, L.; Sheng, G. P.; Liu, J. H.; Yu, H. Q.; Huang, X. J. Enhanced Arsenic Removal from Water by Hierarchically Porous CeO₂-ZrO₂ Nanospheres: Role of Surface- and Structure-Dependent Properties. *J. Hazard Mater.* **2013**, *260*, 498-507.
- (53) Cabelka, T. D.; Austin, D. S.; Johnson, D. C. Electrocatalytic Oxidation of As(III) .1. Voltammetric Studies at Pt Electrodes in 0.5m HClO₄. *J. Electrochem. Soc.* **1984,** *131,* 1595-1602.
- (54) Williams, D. G.; Johnson, D. C. Pulsed Voltammetric Detection of Arsenic(III) at Platinum Electrodes in Acidic Media. *Anal. Chem.* **1992**, *64*, 1785-1789.
- (55) Sumino, M. P.; Shibata, S. Specific Adsorption of Hydrogen on Polycrystalline Platinum Electrode. *Electrochim. Acta* **1992**, *37*, 2629-2635.
- (56) Umeda, M.; Kokubo, M.; Mohamedi, M.; Uchida, I. Porous-Microelectrode Study on Pt/C Catalysts for Methanol Electrooxidation. *Electrochim. Acta* **2003**, *48*, 1367-1374.
- (57) Bensalem, A.; Muller, J. C.; Bozonverduraz, F. From Bulk CeO₂ to Supported Cerium Oxygen Clusters a Diffuse Reflectance Approach. *J. Chem. Soc. Faraday T.* **1992,** *88*, 153-154.
- (58) Everett, K. G.; Skoog, D. A. Uncatalyzed Oxidation of Arsenic(III) by Cerium(IV) in Perchloric Acid Medium. *Anal. Chem.* **1971**, *43*, 1541-1547.
- (59) Li, Z.; Deng, S.; Yu, G.; Huang, J.; Lim, V. C. As(V) and As(III) Removal from Water by a Ce—Ti Oxide Adsorbent: Behavior and Mechanism. *Chem. Eng. J.* **2010**, *161*, 106-113.
- (60) Hirano, M.; Kato, E. Hydrothermal Synthesis of Cerium(IV) Oxide. *J. Am. Ceram. Soc.* **1996,** *79*, 777-780.
- (61) Terribile, D.; Trovarelli, A.; Llorca, J.; de Leitenburg, C.; Dolcetti, G. The Synthesis and Characterization of Mesoporous High-Surface Area Ceria Prepared Using a Hybrid Organic/Inorganic Route. *J. Catal.* **1998**, *178*, 299-308.
- (62) Xu, J. H.; Harmer, J.; Li, G. Q.; Chapman, T.; Collier, P.; Longworth, S.; Tsang, S. C. Size Dependent Oxygen Buffering Capacity of Ceria Nanocrystals. *Chem. Commun.* **2010**, *46*, 1887-1889.

- (63) Beche, E.; Charvin, P.; Perarnau, D.; Abanades, S.; Flamant, G. Ce 3d XPS Investigation of Cerium Oxides and Mixed Cerium Oxide (Ce_xTi_vO_z). *Surf. Interface Anal.* **2008**, *40*, 264-267.
- (64) Wang, T.; Yang, W. C.; Song, T. T.; Li, C. F.; Zhang, L. Y.; Wang, H. Y.; Chai, L. Y. Cu Doped Fe₃O₄ Magnetic Adsorbent for Arsenic: Synthesis, Property, and Sorption Application. *RCS Adv.* **2015**, *5*, 50011-50018.
- (65) Chen, B.; Zhu, Z.; Ma, J.; Qiu, Y.; Chen, J. Surfactant Assisted Ce–Fe Mixed Oxide Decorated Multiwalled Carbon Nanotubes and their Arsenic Adsorption Performance. *J. Mater. Chem. A* **2013**, *1*, 11355-11367.
- (66) Sakthivel, T. S.; Das, S.; Pratt, C. J.; Seal, S. One-pot Synthesis of a Ceria-Graphene Oxide Composite for the Efficient Removal of Arsenic Species. *Nanoscale* **2017**, *9*, 3367-3374.
- (67) Huo, L.; Zeng, X.; Su, S.; Bai, L.; Wang, Y. Enhanced Removal of As (V) from Aqueous Solution Using Modified Hydrous Ferric Oxide Nanoparticles. *Sci. Rep.* **2017**, *7*, 40765.
- (68) Vadahanambi, S.; Lee, S.-H.; Kim, W.-J.; Oh, I.-K. Arsenic Removal from Contaminated Water Using Three-Dimensional Graphene-Carbon Nanotube-Iron Oxide Nanostructures. *Environ. Sci. Technol.* **2013**, *47*, 10510-10517.
- (69) Kwon, S. J.; Zhou, H.; Fan, F.-R. F.; Vorobyev, V.; Zhang, B.; Bard, A. J. Stochastic Electrochemistry with Electrocatalytic Nanoparticles at Inert Ultramicroelectrodes—Theory and Experiments. *Phys. Chem. Phys.* **2011**, *13*, 5394-5402.
- (70) Daryanavard, N.; Zare, H. R. Single Palladium Nanoparticle Collisions Detection through Chronopotentiometric Method: Introducing a New Approach to Improve the Analytical Signals. *Anal. Chem.* **2017**, *89*, 8901-8907.
- (71) Kempahanumakkagari, S.; Deep, A.; Kim, K.-H.; Kumar Kailasa, S.; Yoon, H.-O. Nanomaterial-Based Electrochemical Sensors for Arsenic A review. *Biosens. Bioelectron.* **2017**, *95*, 106-116.

Table of content (TOC)

